Nuclear Inst. and Methods in Physics Research, A 975 (2020) 164201

Contents lists available at ScienceDirect

Nuclear Inst. and Methods in Physics Research, A

journal homepage: www.elsevier.com/locate/nima

Fast-neutron response of $LaBr_3$(Ce) and $LaCl_3$(Ce) scintillators

M.P. Taggart [a,*,1], J. Henderson [b,1]

[a] Department of Physics, University of Surrey, Guildford, Surrey, UK
[b] Lawrence Livermore National Laboratory, Livermore CA 94550, USA

ARTICLE INFO

Keywords:
Neutron detection
Silicon photomultiplier
Lanthanum bromide
Lanthanum chloride

ABSTRACT

The response of $LaBr_3$(Ce) and $LaCl_3$(Ce) scintillators to fast neutrons is investigated. Neutron-induced charged-particle reactions are observed in both materials when exposed to the fast neutrons produced by an AmBe source, with pulse-shape discrimination used to separate channels. $LaBr_3$(Ce) is found to have the best separation between reaction channels, while $LaCl_3$(Ce) has a significantly higher efficiency.

1. Introduction

Lanthanum-halide scintillation detectors, such as $LaCl_3$(Ce) and $LaBr_3$(Ce), have been employed for many years in both fundamental and applied physics due to their excellent γ-ray resolution and fast response (see, e.g. Refs. [1–5]). Here, we identify a previously unreported feature of both of these detectors, namely a response to fast neutrons that can be distinguished using standard pulse-shape discrimination (PSD) techniques. Such a response, coupled with their well-known γ-ray detection capabilities, opens the possibility of using these scintillators for the extraction of spectroscopic neutron and γ-ray data within a single detection medium.

Neutron-induced charged-particle reactions, such as (n, p) and (n, α), result in the creation of a charged particle with kinetic energy

$$E_{kin} = \frac{Q + E_n}{1 + m_x/m_X}, \quad (1)$$

where Q is the Q-value of the reaction, E_n is the energy of the incident neutron, m_x is the mass of the emitted particle and m_X the mass of the residual nucleus following emission. In general $m_x \ll m_X$ and the denominator is therefore approximately unity. The energy deposited in a scintillator following such a reaction on one of its constituent nuclei can thus readily be corrected for a known Q value in order to provide neutron-energy information. Given sufficient resolution for the detection of the produced charged-particle, this can then be used to determine an incident neutron spectrum, without, for example, requiring time-of-flight information as used in e.g. Ref [6].

Relevant neutron-induced charged-particle reaction cross-sections for isotopes of La, Cl and Br are summarised in Fig. 1, as determined in the ENDF-VIII reaction cross-section evaluation [7]. Of the cross-sections relevant to the present work, ^{35}Cl(n,p) and ^{35}Cl(n, α) are clearly largest, and further enhanced in practice by the relatively large (~76%) natural abundance of ^{35}Cl. The ^{79}Br(n,p) channel is also relatively strong, albeit an order-of-magnitude reduced from the aforementioned ^{35}Cl reactions. All other reactions are significantly less influential due to their lower cross-sections or limited natural abundance (e.g. ^{37}Cl(n, α) and ^{37}Cl(n,p)).

Based on the above cross-section information, one would expect $LaCl_3$(Ce) to have a superior efficiency for the detection of fast neutrons ($E \gtrsim 1$ MeV), with $LaBr_3$(Ce) having an efficiency about an order of magnitude lower. On the other hand, the energy resolution of $LaBr_3$(Ce) is notably superior to that of $LaCl_3$(Ce).

2. Methods

A scintillator-SiPM (silicon photomultiplier) device was constructed and exposed to various radiation sources. γ-ray calibrations were performed using ^{22}Na, ^{60}Co, ^{137}Cs, and ^{152}Eu sources whereas the mixed radiation field was provided by an 18.5 GBq ^{241}AmBe neutron source. Measurements with the AmBe source were performed overnight for 17 hours, whereas calibration data was taken until sufficient statistics were acquired.

2.1. Scintillators

Scintillators of identical geometry were purchased (Shalom EO, China), a sample of lanthanum chloride ($LaCl_3$) to investigate the chlorine content of the material, and a piece of lanthanum bromide ($LaBr_3$) to act as a comparison. Both materials were doped with cerium at a concentration of 5% mol as specified by the manufacturer. Each scintillator crystal was 1 cm^3 and fully encapsulated in an aluminium casing due to the hygroscopy of the material (see Fig. 2). The scintillator was coupled to the photodetector using Dow Corning high vacuum silicone grease to maximise optical transmission.

* Corresponding author.
E-mail addresses: m.taggart@surrey.ac.uk (M.P. Taggart), henderson64@llnl.gov (J. Henderson).
[1] Both authors contributed equally to this work.

https://doi.org/10.1016/j.nima.2020.164201
Received 13 April 2020; Received in revised form 27 May 2020; Accepted 28 May 2020
Available online 2 June 2020

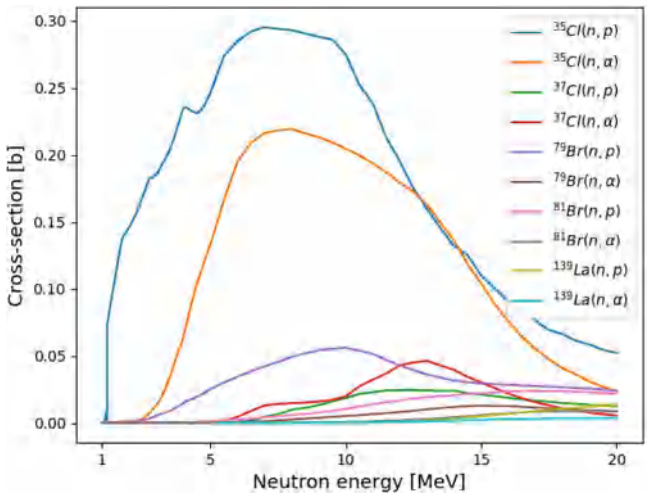

Fig. 1. Neutron-induced charged particle reactions for relevant nuclides within $LaCl_3$(Ce) and $LaBr_3$(Ce) according to the ENDF-VIII evaluation [7] (Colour online). Reactions on ^{35}Cl dominate all others by approximately an order of magnitude or more. The ^{79}Br(n,p) is the next most important to consider.

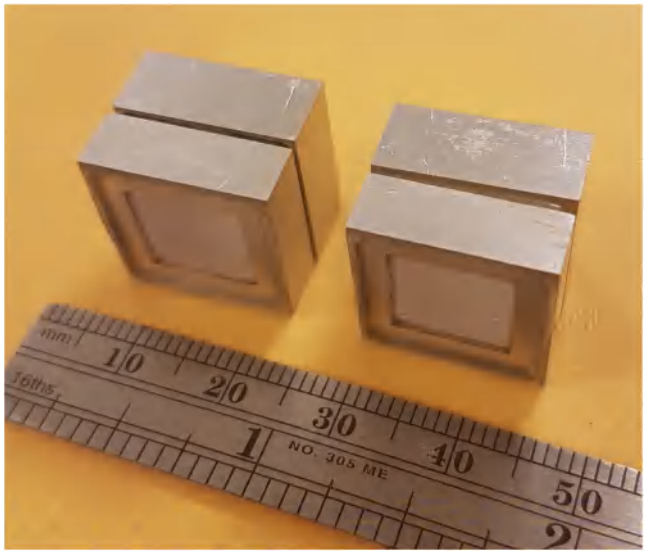

Fig. 2. The encapsulated $LaBr_3$ (left) and $LaCl_3$ (right) scintillators.

2.2. Silicon photomultiplier

A 2 × 2 array of SensL 6 mm^2 J-series SiPMs was selected as the photodetector to fully capture the emission from the scintillator. Previous investigations had established 27.3 V as an appropriate operating voltage [8], equivalent to an overvoltage of 2.5 V, which was supplied using a CAEN N1419 PSU.

2.3. Data acquisition

The output of the detector was immediately digitised using a CAEN V1730C. The digitiser has an ADC resolution of 14-bits, covering a selectable analogue dynamic range of 0.5 V or 2 V, a sample rate of 500 MS/s, and a bandwidth of 250 MHz. All data were processed offline using a ROOT [9] analysis code.

2.4. Analysis

The charge comparison method of pulse shape discrimination is a widely known technique [10,11], whereby two time gates are applied over a pulse, and the charge contained within each is integrated. For this work, best results were found with a short gate duration of 150 ns, with the total pulse recorded with a 760 ns window. The ratio of these two integrals (referred to henceforth as the PSD parameter) can be plotted against the total charge in the pulse to identify different interactions with sensitivity to the ionisation density of the interacting particle.

To elucidate the fast neutron response of the materials we acquired data with the $LaBr_3$(Ce) and $LaCl_3$(Ce) scintillation detectors in three irradiation configurations, with the same exposure time (17 hours). In the first ("thermal") configuration, the AmBe source was shielded from the detector by 30 cm of water, allowing the neutrons to thermalise before interacting with the detector. In the second ("fast"), the setup remained identical, but the water was displaced with a hollow "air tube", dramatically reducing thermalisation of neutrons. In both cases, the detector was additionally shielded by a lead brick to reduce exposure to γ rays. Data were also acquired ("background") without exposure to a source, providing a measure of the internal and room backgrounds.

Fig. 3 shows the PSD parameter plotted against the calibrated energy for the three configurations for $LaCl_3$(Ce) and $LaBr_3$(Ce), with a some features immediately apparent. Note that the PSD response is inverted between the two materials, with higher ionisation density resulting in a larger PSD value for $LaCl_3$(Ce) and a smaller value in $LaBr_3$(Ce). Average 1/e decay times, convoluted with the acquisition electronics and the SiPM readout circuitry, were recorded as: 427.6(6.2), 450.2(5.3), and 483.5(7.8) ns for $LaCl_3$, and 285(3.4), 272.2(2.5), and 259.4(2.2) ns for $LaBr_3$ (times for γ ray, proton, and α pulses respectively). As is clear from the background measurements, both detectors contain an α-decaying contamination. This is a well-known property of lanthanum-halides and originates from long-lived actinium contamination [12]. Comparison of the fast and thermal spectra shows some clear excess counts in the PSD dimension. In the $LaBr_3$(Ce) spectra (Fig. 3, right), three loci are clearly distinguished, with the new locus lying between γ rays and α particles. This indicates energy deposition by an interacting particle with an intermediate ionisation density to γ rays and α particles: protons. A similar feature is seen in the $LaCl_3$(Ce) data (Fig. 3, left), albeit with an inferior separation. Indeed, the proton events here appear as a shoulder on the γ-ray distribution. No indication of events in these regions is found in the background data, with a greatly reduced number of counts in the thermal data as compared to the fast. We can therefore identify these events as originating from (n,p) reactions induced by fast neutrons. Some additional events also appear in the region of the α-locus, indicating that an (n,α) channel is also active.

3. Discussion

In order to extract a spectrum of the proton and α energies in $LaCl_3$(Ce) the proton shoulder needed to be extracted. This was done by projecting the data shown in Fig. 3 along the PSD axis and performing a triple-Gaussian fit. An example fit is shown in Fig. 4, where the individual contributions (dashed lines) can be extracted by integrating each distribution to determine the number of γ-ray, proton and α-particle events at that energy. The areas of the respective γ-ray, proton and α-particle peaks are shown in Fig. 5 plotted against the calibrated energy for both the thermal and fast data. The γ-ray spectrum is similar for both, albeit slightly attenuated in the thermal data as compared to the fast. In the α-particle spectrum the contaminant peaks dominate both fast and thermal data, however there is a clear excess in the fast spectrum at energies lower than the contaminant, with some small excess at higher energies as well. The proton spectrum is almost completely suppressed in the thermal data, whereas in the fast data significant contributions are observed. Within the 1000 keVee to 5000 keVee range 2090(80) proton counts are observed in the fast data, as compared to 212(65) events in the thermal data.

In the $LaBr_3$(Ce), the PSD separation is excellent. Protons, α particles, and γ rays are well separated with the respective loci discernible

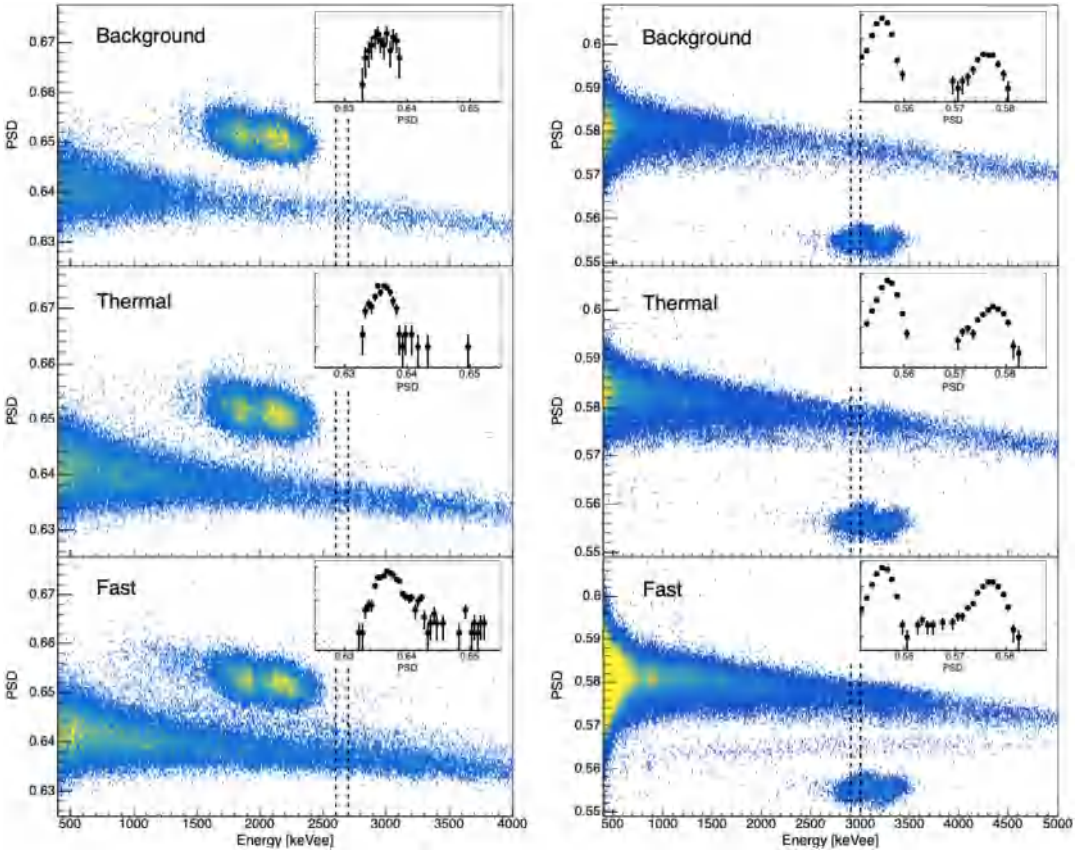

Fig. 3. Pulse-shape discrimination parameter, PSD, plotted against the energy measured in the $LaCl_3$(Ce) (left) and $LaBr_3$(Ce) (right) detectors for (top) internal and room backgrounds, (middle) exposure to thermal neutrons and (bottom) exposure to fast neutrons. See text for details. Regions of counts are clearly visible in the fast neutron data between the γ and α particle loci that is not strongly present in either the thermal or background data. The inset figures are projections on the PSD axis performed in the region indicated by the dashed lines, demonstrating the additional response to fast neutrons.

by eye in Fig. 3. No significant excess was observed for α particles, as expected from the cross-sections shown in Fig. 1. Fig. 6 shows the resultant spectra, following the same analysis as performed for the $LaCl_3$(Ce). Between 1000 keVee and 5000 keVee, 404(23) protons were observed in the fast spectrum, as compared to 28(7) in the thermal data. Note that the ratio of thermal to fast neutrons is consistent in both $LaBr_3$(Ce) and $LaCl_3$(Ce), within 1σ uncertainties.

The PSD properties of a material can be quantified by a figure-of-merit (FOM) [13], defined as

$$FOM = \frac{|C(x) - C(y)|}{|\Gamma(x) + \Gamma(y)|}, \tag{2}$$

where x and y are the particle types being differentiated (proton, γ-ray or α-particle), C corresponds to the centroid of that particle type and Γ is the full-width at half-maximum of the distribution of that particle type. The FOM values for $LaCl_3$(Ce) and $LaBr_3$(Ce) determined in the present work are given in Figs. 7 and 8 respectively, plotted against the electron-equivalent energy. The separation between α particles and γ rays in $LaCl_3$(Ce) is consistently good, with a FOM greater than 1.5 at most energies, while protons and α particles are relatively well-separated (FOM $\sim$1). Proton-γ separation is less pronounced, with a FOM value of approximately 0.5 at all energies. In $LaBr_3$(Ce) there is no significant detection of α-like events outside of the contaminant region, and so α-γ and proton-α FOMs are only shown in the contaminant region. The proton-γ differentiation is good, with $FOM > 1.26$ at low energies, indicating a separation of better than 3σ. At higher energies the proton and γ like events become less well separated, which can be seen in the bottom panel of Fig. 3 (right). We note a significantly improved PSD in $LaBr_3$(Ce) as compared to that given in, for example, Ref. [14]. This is likely due to the considerably smaller volume used in the present work [15]: 1 cm^3 here, as compared to ∅1“x1” (12.9 cm^3) in Ref. [14].

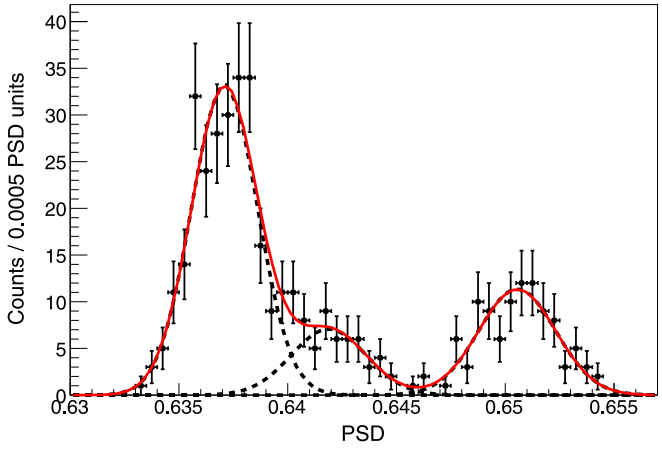

Fig. 4. An example fit to the $LaCl_3$(Ce) PSD values with a triple-Gaussian with the individual contributions shown. Peaks, from left to right, correspond to γ rays, protons and α particles.

The phenomenon of spectrum “quenching”, whereby particles with larger linear-energy transfer (LET) induce a proportionally lower scintillation signal than those with a lower LET value has previously been described in, for example, $LaBr_3$(Ce) [16,17]. It can clearly be seen in the α-particle contamination of Fig. 3, where the highest energy peak (7386 keV from ^{215}Po α decay) is quenched to an electron-equivalent

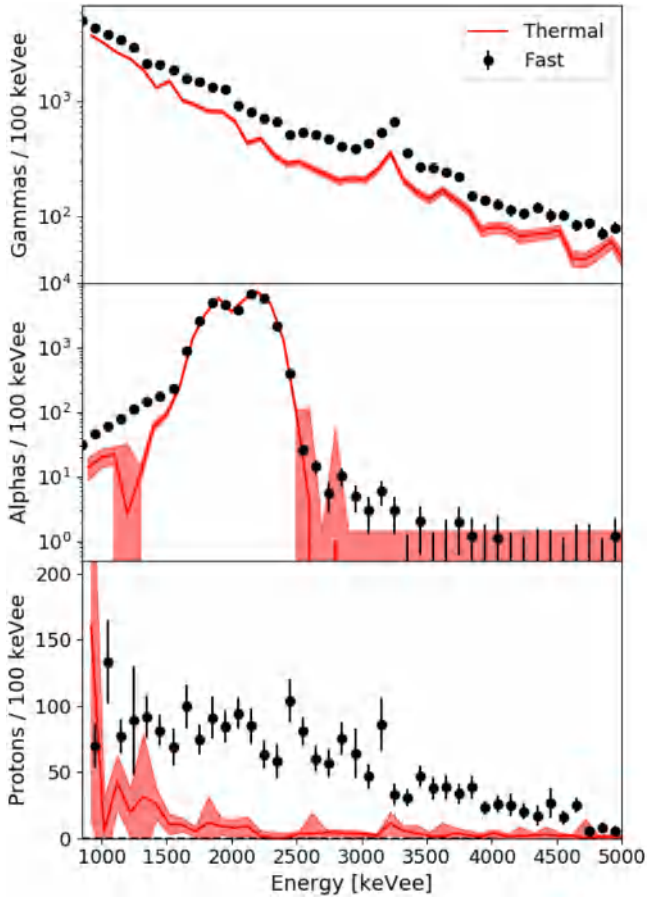

Fig. 5. Fast (black points) and thermal (red line and uncertainty band) energy spectra for (top) γ rays, (middle) α particles and (bottom) protons in $LaCl_3$. Clear excesses are seen in both the α-particle and proton spectra due to (n,p) and (n,α) reactions. The peak in the γ-ray spectrum corresponds to the double-escape peak originating from the 4.4 MeV decay of the first-excited state in ^{12}C.

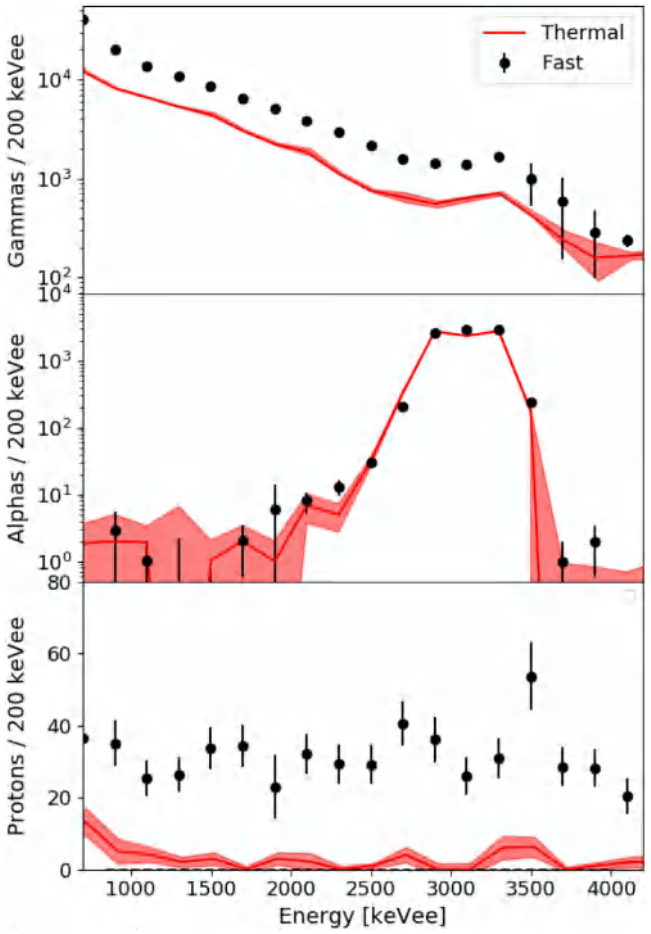

Fig. 6. As Fig. 5 but for $LaBr_3$. No enhancement is seen in the α spectrum, as expected from the reduced cross section. Note that coarser binning is used than in Fig. 5 due to the reduced statistics.

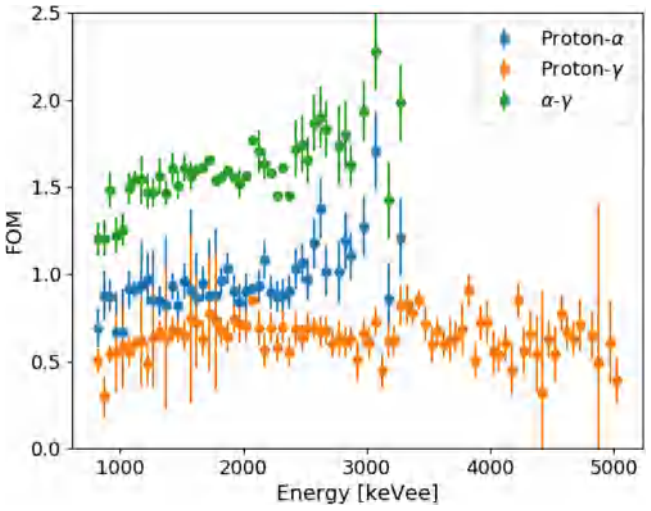

Fig. 7. Figure of merit for $LaCl_3$(Ce) showing the separation in PSD between protons and α particles, protons and γ rays and α particles and γ rays.

energy of approximately 2300 keVee in $LaCl_3$(Ce) and approximately 3400 keVee in $LaBr_3$(Ce). The energy spectra presented in Figs. 5 and 6 are the quenched spectra, with the α-particle spectrum expected to experience more quenching than the corresponding proton spectrum.

Interpretation of the experimental data was aided by simulations of the detectors' response to fast-neutron exposure in GEANT4 [18]. The experimental AmBe neutron spectrum of Ref. [19] was used, with the experimental setup simulated and repeated for both the $LaBr_3$(Ce) and $LaCl_3$(Ce) crystals. The simulations incorporated the (n,p) and (n,α) cross sections shown in Fig. 1. Based on these simulations it is expected that (n,p) reactions on $LaBr_3$(Ce) will have an efficiency approximately 6% that of (n,p) reactions in $LaCl_3$(Ce). Due to uncertainties in the quenching of the proton pulse height a direct comparison of simulation to data is not possible, however the number of proton-like events detected experimentally in the $LaBr_3$(Ce) between 1000 keVee and 5000 keVee is found to be approximately 20% that of $LaCl_3$(Ce) within the same range, perhaps indicating some deficiency in the cross-sections of Fig. 1.

4. Conclusions

We have demonstrated the fast-neutron response of two common lanthanum-halide detectors: $LaCl_3$(Ce) and $LaBr_3$(Ce). Neutrons interact with the scintillator by (n,p) and (n,α) reactions, resulting in charged-particles depositing energy in the material and giving direct access to the incident neutron energy. It is found that both scintillation materials have pulse-shape discrimination (PSD) properties for γ-rays, protons and α particles. $LaBr_3$(Ce) demonstrates exceptional PSD with γ rays, protons and α particles clearly separated. $LaCl_3$(Ce) meanwhile has reduced separation, requiring a more intensive analysis to extract a neutron spectrum. Given that $LaCl_3$(Ce) has a considerably higher

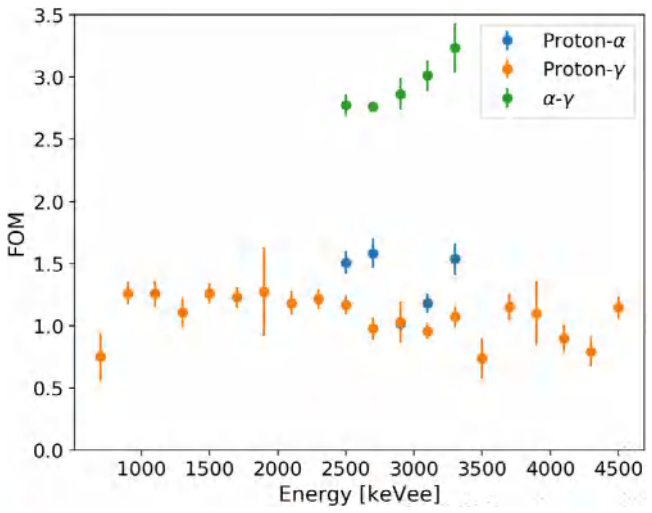

Fig. 8. Figure of merit for $LaBr_3$(Ce) showing the separation in PSD between protons and α particles, protons and γ rays and α particles and γ rays. Note that for the α particle separations only the energy region corresponding to the actinium contamination is included due to poor statistics elsewhere.

efficiency for the detection of neutrons it would be of great interest to develop the material's PSD properties further.

CRediT authorship contribution statement

M.P. Taggart: Conceptualization, Methodology, Investigation, Writing - review & editing. **J. Henderson:** Conceptualization, Formal analysis, Writing - original draft.

Declaration of competing interest

The authors declare that they have no known competing financial interests or personal relationships that could have appeared to influence the work reported in this paper.

Acknowledgements

MPT would like to acknowledge the STFC Nuclear Security Science Network (NuSec). Work at LLNL was performed under contract DE-AC52-07NA27344.

References

[1] M. Tsutsumi, Y. Tanimura, Nucl. Instrum. Methods Phys. Res. A 557 (2005) 554–560.
[2] S. Zhu, F. Kondev, M. Carpenter, I. Ahmad, C. Chiara, J. Greene, et al., Nucl. Instrum. Methods Phys. Res. A 652 (1) (2011) 231–233, http://dx.doi.org/10.1016/j.nima.2010.10.059, http://www.sciencedirect.com/science/article/pii/S0168900210023211.
[3] O.J. Roberts, A.M. Bruce, P.H. Regan, Z. Podolyák, C.M. Townsley, J.F. Smith, et al., Nucl. Instrum. Methods Phys. Res. A 748 (2014) 91–95, http://dx.doi.org/10.1016/j.nima.2014.02.037, http://www.sciencedirect.com/science/article/pii/S0168900214002137.
[4] J. Tain, J. Agramunt, A. Algora, A. Aprahamian, D. Cano-Ott, L. Fraile, et al., Nucl. Instrum. Methods Phys. Res. A 774 (2015) 17–24, http://dx.doi.org/10.1016/j.nima.2014.11.060, http://www.sciencedirect.com/science/article/pii/S0168900214013485.
[5] M. Zeng, J. Cang, Z. Zeng, X. Yue, J. Cheng, Y. Liu, et al., Nucl. Instrum. Methods Phys. Res. A 813 (2016) 56–61, http://dx.doi.org/10.1016/j.nima.2015.12.045, http://www.sciencedirect.com/science/article/pii/S0168900215016253.
[6] W. Peters, S. Ilyushkin, M. Madurga, C. Matei, S. Paulauskas, R. Grzywacz, et al., Nucl. Instrum. Methods Phys. Res. A 836 (2016) 122–133, http://dx.doi.org/10.1016/j.nima.2016.08.054, http://www.sciencedirect.com/science/article/pii/S0168900216308816.
[7] D.A. Brown, M. Chadwick, R. Capote, A. Kahler, A. Trkov, M. Herman, et al., Nucl. Data Sheets 148 (2018) 1.
[8] M.P. Taggart, P.J. Sellin, Nucl. Instrum. Methods Phys. Res. A 908 (2018) 148–154.
[9] R. Brun, F. Rademakers, Nucl. Instrum. Methods Phys. Res. A 389 (1997) 81–86.
[10] F.D. Brooks, Nucl. Instrum. Methods 4 (1959) 151–163.
[11] G. Ranucci, Nucl. Instrum. Methods Phys. Res. A 354 (1995) 389–399.
[12] G.F. Knoll, Radiation detection and measurement / Glenn F. Knoll, fourth ed., Wiley New York, 2010, p. 251 p..
[13] R.A. Winyard, J.E. Lutkin, G.W. McBeth, Pulse shape discrimination in inorganic and organic scintillators I, Nucl. Instrum. Methods 95 (1971) 141–153.
[14] K. Yang, P.R. Menge, V. Ouspenski, 2014 IEEE Nuclear Science Symposium and Medical Imaging Conference (NSS/MIC), 2014, pp. 1–5, http://dx.doi.org/10.1109/NSSMIC.2014.7431223.
[15] M. Ellis, C. Tintori, P. Schotanus, K. Duroe, P.A. Kendall, G. Mini, The effect of detector geometry on EJ-309 pulse shape discrimination performance, in: 2013 IEEE Nuclear Science Symposium and Medical Imaging Conference (2013 NSS/MIC), 2013, pp. 1–6.
[16] A. Miller, R. Machrafi, A. Fariad, Radiat. Meas. (ISSN: 1350-4487) 115 (2018) 43–48, http://dx.doi.org/10.1016/j.radmeas.2018.06.009, http://www.sciencedirect.com/science/article/pii/S1350448717306030.
[17] N. Matsufuji, T. Kanai, H. Komami, T. Kohno, Nucl. Instrum. Methods Phys. Res. A 430 (1999) 60–68.
[18] S. Agostinelli, J. Allison, K. Amako, J. Apostolakis, H. Araujo, P. Arce, et al., Nucl. Instrum. Methods Phys. Res. A 506 (2003) 250–303, http://dx.doi.org/10.1016/S0168-9002(03)01368-8, http://www.sciencedirect.com/science/article/pii/S0168900203013688.
[19] J.W. Marsh, D.J. Thomas, M. Burke, Nucl. Instrum. Methods Phys. Res. A 366 (1995) 340–348.